19

Novel Approaches for SER Spectroscopic Analysis of Protein Cofactors

Sezer Murat, Sivanesan Arumugam,
Feng Jiu-Ju and Weidinger Inez M.
Technische Universität Berlin
Henan Normal University
Germany
China

1. Introduction

Biomimetic systems employed for biotechnological applications i.e. as biosensors or bio fuel cells, require initial formation of conducting support/protein complexes with controlled properties. The specific interaction of the protein with the support determines important qualities of the device such as electrical communication, long-term stability and catalytic efficiency. In this respect the system parameters have to be chosen in a way that high protein loading on the support is achieved while protein denaturation upon adsorption is prevented. The conditions on the surface have to be adjusted in such a way that the desired surface reaction of the protein i.e. electron transfer to either the electrode or a second redox partner, is still guaranteed. Hence the choice of support, its functionlisation as well as the right adjustment of solution parameters play a crucial role in the rational design of these support/protein constructs.

Optical spectroscopy on surface bound proteins can give insight into the molecular processes that occur at the protein/support interface and thus represent a powerful addition to electrochemical methods that monitor the integrated response of surface active species only. However, optical spectroscopy in general lacks surface sensitivity which is necessary to detect the small amounts of proteins that are attached to the surface. Surface sensitivity can be obtained if the conducting support is able to create surface plasmon resonances (SPRs) generated by the resonant interaction of light with the free electron gas of a metal support. The SPR enhances the electromagnetic field in close vicinity of the metal surface which in turn amplifies the optical signal of surface bound molecules.

The most widely used spectroscopic technique that makes use of plasmonically enhanced electric fields is *surface enhanced Raman spectroscopy* (SERS). In general with Raman spectroscopy unique vibrational fingerprints of target molecules can be obtained; hence SERS is mostly applied in analytical surface chemistry (Smith, 2008). In life science SER spectroscopy can be used to monitor the structural state of immobilized proteins during surface reactions (Siebert & Hildebrandt, 2008). A key role in such reactions is played by protein cofactors that act as active centres i.e. for electron transfer or catalytic substrate conversion. In contrast to the protein matrix many of these cofactors show a strong absorption in the visible light region. If the energy of an exciting laser line is tuned to the

absorption maximum of such a chomophore, the intensity of the Raman scattered light is enhanced by several orders of magnitude for the selective vibrations of the said chomophore. This effect is utilized in *resonance Raman* (RR) spectroscopy, which not only increases the detection sensitivity but also allows to selectively monitoring the chromophoric group of interest in a complex biomolecular construct. If the surface enhancement and molecular resonance effect is combined *surface enhanced resonance Raman spectroscopy* (SERRS) can be a powerful tool to analyse protein cofactors solely of surface bound biomolecules. This selective enhancement however requires a smart tuning of the support's optical properties while at the same time the chemical and electrical optimisation of the system has to be considered.

The choice of support is a clear limitation in SER(R) spectroscopy as only metal supports that exhibit SPRs in the visible region can be considered. This narrows possible choices down to silver (Ag) and gold (Au) supports. While Au is a relative biocompatible metal, which is commonly used in electrochemical investigations of redox enzymes (Leger & Bertrand, 2008), Ag is generally considered as toxic and chemically instable. However, regarding its optical properties Ag is clearly superior to Au since it exhibits higher surface enhancement and its SPR can be tuned from near UV to infrared (Le Ru & Etchegoin, 2009). The SER activity of Au on the other hand is restricted to wavelengths larger than 520 nm which makes this metal not suitable for SERR spectroscopic investigations of chromophores that absorb in the blue and violet region.

Within the limits given by the metal support the position and magnitude of an SPR can be furthermore tuned by changing the surface morphology and the dielectric constant of the surrounding medium. Monodisperse nanoparticles show defined SPRs normally in the size range between 10 and 100 nm. As a rule of thumb the SPR position for nanoparticles is red-shifted with increasing diameter and aspect ratio, which is defined as the ratio between the longer and the shorter axis of the particle. It is further red-shifted with increasing dielectric constant of the surrounding medium (Kelly et al. 2003; Link & El-Sayed, 1999). Metal aggregates generally exhibit higher field enhancement than isolated nanostructures due to plasmonic interaction between the nanoscopic subunits. Moreover their SPR position is significantly red-shifted (Lal et al., 2008; Prodan et al., 2003).

For biological applications the influence of the metal on the biomolecule has to be considered as the interaction with bare metal surfaces usually denaturates proteins. In order to retain the native structure of the protein upon adsorption the metal has to be coated with a biocompatible material. Such coatings can be made of *self assembled monolayers* (SAMs) of ω-functionalised mercaptoalkanes (Bain et al., 1989). The thiol group interacts with the metal surface forming a stable covalent bond. The functionalisation of the head group that faces the solution can be varied and is generally chosen in respect to the protein under investigation. However, the properties of organic SAMs are metal-specific such that results obtained with Ag can not generally be transferred to other support materials. Thus a major challenge for SERR spectroscopic applications remains to combine the specific optical requirements of the support material with conditions optimised for biotechnological applications. The aim of this book chapter is to present several approaches how selective enhancement of protein cofactors can be achieved using different support architectures and immobilisation strategies and to discuss the respective advantages and disadvantages in respect to applications in bioanalysis.

2. Methology

In SERR spectroscopy of protein cofactors the following steps have to be considered: First the support material for optical amplification has to be chosen and its SPR has to be tuned in respect to the protein cofactor under investigation. Second, a surface functionalisation has to be chosen that guarantees protein adsorption in a defined orientation and preservation of the protein´s native state. Third, solution parameters like pH and ionic strength have to be adjusted for optimum functionality of the protein in respect to i.e. electrical communication and/or catalytic activity.

Heme cofactors are found in a variety of proteins with a broad range of functions. One of its main functions is found in electron transport reactions as the central Fe-ion of the heme can easily be reduced or oxidised. Hemes show strong absorption in the Soret region around 410 nm which makes them highly visible in RR spectroscopy (Siebert & Hildebrandt, 2008) Excitation with a 413 nm line of a Krypton ion laser is in this case the method of choice to selectively monitor the structural state of the heme. The vibrational pattern obtained in this way is characteristic for the redox and conformational state of the heme. Thus redox reactions and/or changes in axial ligation of the heme iron can be precisely monitored. The latter allows distinguishing heme cofactors of different protein complexes and, even more important, following denaturation processes that go along with changes of the axial ligation pattern. As a drawback SERR analysis of heme cofactors requires surface enhancement upon violet light excitation which can only be achieved using Ag as amplifying support. Several aspects have to be taken into account for designing the appropriate SER active support:

The enhancement of the Raman scattered light *REF* is the product of the field enhancement intensity at the wavelength of the exciting $EF(\lambda_{exc})$ and Raman scattered $EF(\lambda_{Ra})$ radiation.

$$REF = EF(\lambda_{exc}) \cdot EF(\lambda_{Ra}) \tag{1}$$

Hence maximum SERR intensity is expected when the SPR maximum lies somewhere in between λ_{exc} and λ_{Ra}.

Additionally, the Raman enhancement *REF* shows a strong dependence on the distance from the SER active surface. For a spherical nanoparticle in a homogeneous medium this distance dependence can be described by:

$$REF(d) = REF(0) \cdot \left(\frac{a_0}{a_0 + d} \right)^{12} \tag{2}$$

where a_0 is the radius of the nanoparticle, d is the distance of the Raman scatterer to the metal surface, and *REF(0)* refers to the Raman enhancement factor for the probe molecule in direct contact with the surface.

Monolayers of organic molecules represent the most versatile biocompatible coating material. Attachment of these layers to nanostructured surfaces changes the particle size and the dielectric constant of the surrounding medium and thus results in a shift in SPR that has to be taken into account in the design of smart SERS active supports. Moreover, the organic coating separates the protein from the metal surface which, according to equation 2, can decrease the Raman signal enhancement drastically.

If the SER active support can be utilized as a working electrode in an electrochemical cell, redox titrations of surface bound proteins can be monitored by potential dependent SER(R) spectroscopy. The redox state of the protein cofactor is in this case followed as a function of

applied potential. Moreover electrochemical methods can be employed on the same system that give additional and often complementary information.
Time resolved SER(R) spectroscopy (Tr-SER(R)S) can be used to study the electron transfer dynamics of redox proteins on SER active electrodes. Here the redox equilibrium is disturbed by a potential jump of the working electrode. The relative contribution of the reduced and oxidised state of the protein, as it reaches its new equilibrium, can be followed with SERS as a function of time subsequent to the jump. This allows determining the apparent redox rate of the metal/protein complex also as a function of the reaction´s driving force.

3. SERR active biomimetic systems

As pointed out in section 2, Ag is the only support that can be used as optical amplifier for SERR spectroscopic investigations of heme protein cofactors. However the quantitative yield of the amplification at violet light excitation can change drastically as a function of Ag morphology. In this section several Ag architectures are presented, that can be chosen in respect to the intended application (Figure 1). We start with size-tuned nanoparticles followed by rough electrodes for spectro-electrochemical applications. Last but not least we will introduce multilayered hybrid Ag-Au systems that aim to combine the optical properties of Ag with the chemical advantages of Au.

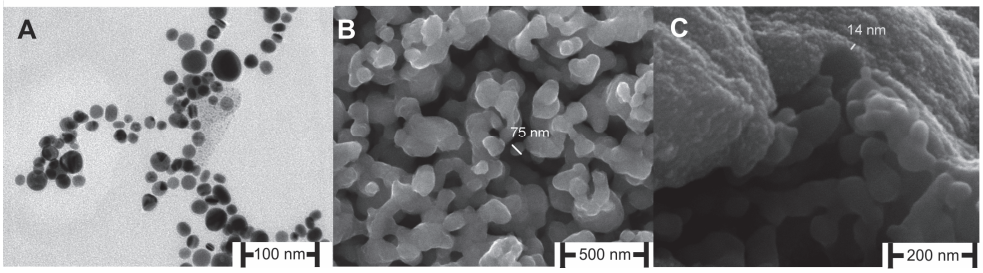

Fig. 1. SEM pictures of different SER active Ag supports: (A) Ag nanoparticles, (B) rough Ag electrodes and (C) layered Ag-Au hybrid electrodes.

3.1 Tunable and biocompatible Ag nanoparticles

Although the SERS effect was discovered on rough electrodes (Jeanmaire & van Duyne 1977), nanoparticles (NPs) were the first systems extensively investigated on their electric field enhancement properties. Isolated monodisperse NP ensembles exhibit very sharp SPRs which can be seen as a resonance absorption in the UV-vis spectrum. The frequency of the SPR maximum strongly depends on the particle's size, its shape and the dielectric properties of the environment. The frequency dependent enhancement factors of spherical and ellipsoidal particles can be determined analytically using Mie scattering theory (Zeman & Schatz, 1987). In general, experimentally determined SPR positions are in very good agreement with the theoretical predictions (Link & El-Sayed, 1999).
AuNPs are widely used for SER investigations since they can be synthesized very homogeneous in size, exhibit a high stability and are commercially available. The use of Ag NPs is less common since they have to be prepared individually and it is much more

difficult to obtain a narrow size distribution (Le Ru & Etchegoin, 2009). For selective enhancement of heme cofactors AgNPs are designed with SPRs that match exactly the Soret band transition of the heme (Sivanesan et al, 2011).

3.1.1 Size adjustement

Small NPs can be prepared by reducing Ag+ ions with borohydride in the presence of citrate. The resulting NPs are quite spherical with an average size of 12 nm and an aspect ratio, defined as the longer *vs.* shorter diameter, of 1.04. Without any further treatment the generated particles show a sharp SPR at 390 nm. In order to tune the SPR so it matches the molecular absorbance of the heme cofactor the particle size has to be further increased. To achieve this, a defined concentration of *silver nitrate* ($AgNO_3$) and *ascorbic acid* is added to the seeds. This seeding method was established for AuNPs (Jana et al., 2001) but also for AgNPs an almost linear correlation between growth solution concentration and either particle size or aspect ratio can be obtained (Sivanesan et al, 2011). As a consequence the SPR position of the nanoparticle ensemble is red-shifted as a function of growth solution concentration. This effect is shown exemplarily for 4 NP batches in figure 2A.

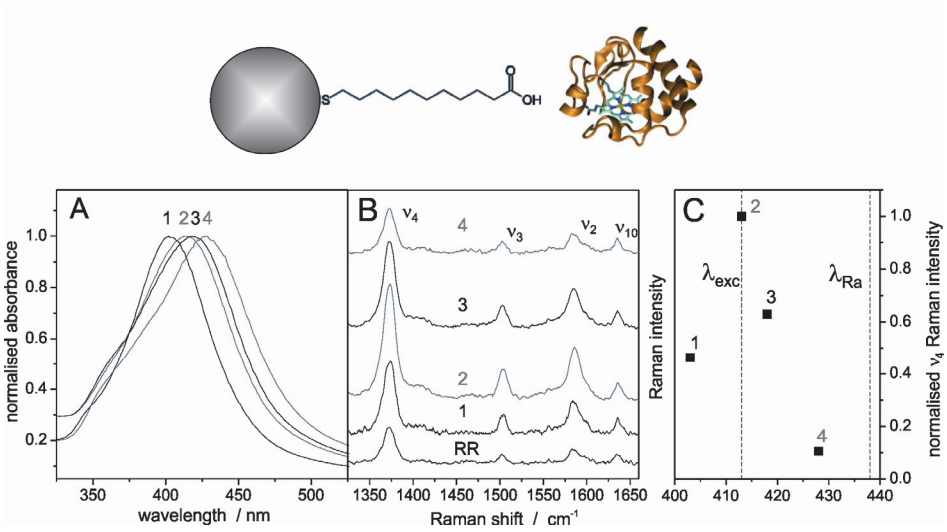

Fig. 2. (A) SPRs of MUA capped AgNPs of different average size. (B) RR and SERR spectra of Cyt *c* in solution and attached to NPs with different SPR maximum. (C) SERR intensity of the ν_4 band of Cyt *c* on different AgNP batches as a function of their respective SPR maximum. The vertical dashed lines mark the wavelength of the laser excitation (λ_{exc}) and the Raman scattered light at the ν_4 position (λ_{Ra}).

3.1.2 Surface functionalisation

The surface of the NPs is initially covered by citrate ions which are known to cause severe protein denaturation (Hildebrandt & Stockburger, 1986). The citrate ions can be replaced by SAMs of ω-functionalised mercaptoalkanes via ligand exchange (Bonifacio et al., 2004). These SAMs have shown to significantly improve the structural integrity of redox proteins

on metal surfaces (Tarlov & Bowden, 1991). SAMs are commercially available with a variety of alkane chain length and functionlisation groups. The latter is chosen individually in respect to the target protein.

Cytochrome c (Cyt *c*) is a small soluble heme protein that acts as a mobile electron carrier in the mitochondrial respiratory chain. It possesses a positively charged lysine rich domain close to the heme cofactor. The protein binds electrostatically via this region to carboxyl-terminated SAMs. Therefore, to achieve biocompatible adsorption of Cyt *c* on AgNPs precedent functionalisation by a carboxylic mercaptoalkane, e.g. *mercaptoundecanoic acid* (MUA, $HS(CH_2)_{10}COOH$), is necessary.

Successful replacement of citrate by MUA is accompanied by a red shift in the plasmon resonance of ca. 14 nm. Subsequent binding of Cyt *c* can also be followed by a further red shift of ca. 8-10 nm. For all NP batches shown in Figure 2A, SERR spectra of Cyt c could be obtained albeit with a different Raman signal enhancement (Figure 2B).

If the monolayer coverage is complete and homogeneous, the vibrational pattern of Cyt c in the SERR spectrum is similar to its RR spectrum indicating that the protein retains in its native structural conformation upon immobilisation. Damaged SAMs or incomplete SAM coverage, as obtained i.e. if too low SAM concentrations are used during NP preparation, alter the SERR spectrum as can be seen i.e. by the formation of an additional band at 1490 cm^{-1} (Figure 3) which is attributed to a non native 5 coordinated high spin state where the 6th axial ligand is missing (Oellerich et al. 2002). At least an excess ratio of 6:1 MUA:NP concentration is needed to obtain exclusively native protein on the surface. However the formation of a biocompatible layer is done on the expense of SERR intensity which drops by roughly one order of magnitude due to the increasing distance of the heme cofactor from the Ag surface by ca. 2 nm.

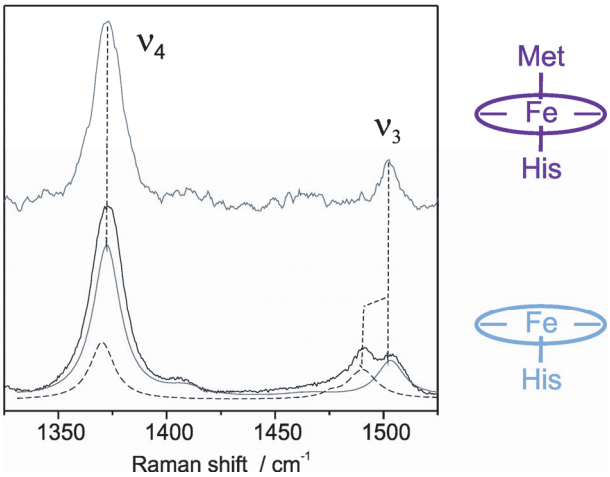

Fig. 3. RR (top) and SERR (bottom) spectrum of ferric Cyt *c* on AgNPs where the MUA coating is not complete. The solid grey and dashed black lines in the lower spectrum represent the respective component spectra of the native low spin and non native high spin species. On the right side the coordination of the heme in its native low spin (top) and non native high spin (bottom) state is shown schematically.

The SERR intensity of the protein shows a strong dependence on the SPR position as can be seen in figure 2 C. A clear intensity maximum is seen for the NP ensemble with a maximum SPR at 413 nm which matches both, the laser line (413 nm) and the molecular absorption maximum of oxidised Cyt c (410 nm), best. NPs with higher or lower SPR maximum show much lower SERR intensities. This clearly demonstrates that efficient enhancement is only achieved in the very narrow frequency range where laser excitation, NP plasmon resonance and molecular absorption of the chromophore overlap.
If the particle size and the Cyt *c* surface coverage are known, the Raman signal enhancement factor (*REF*) can be directly calculated from the Cyt *c* SERR intensity. For the 413 nm NP batch *REF* was thus determined to be 130 at the MUA/protein interface. If we correct this value for the signal attenuation caused by the thickness of the MUA layer and by applying equation 1 we obtain *EF*(413 nm) = 37 directly at the Ag surface. This result fits very nice to the theoretical predicted *EF* factor of 40 (Zeman & Schatz, 1987), which presents an upper limit for experimental determined enhancement factors since it was calculated under the premise that the frequency of the incoming light and the SPR maximum are identical.

3.2 Spectro-electrochemistry of heme proteins on rough Ag electrodes

Enhanced electromagnetic fields via surface plasmon resonances can also be generated by nanostructured electrodes. These electrodes can additionally function as working electrodes in an electrochemical cell. Thus by applying an external potential the metal support may serve as an electron supply or sink for electron transfer reactions of immobilised redox proteins.
A nanostructured electrode can be seen as an ensemble of connected nanoparticles. Due to the plasmonic coupling of the individual nano-units the intensity and position of the electrode's SPR is significantly altered as a function of surface morphology. Lithographic methods can be used to create highly periodic nanostructures with distinct plasmonic properties (Haynes & Van Duyne, 2001); the setup of such devices is, however, very expensive. Electrochemical methods on the other hand can be performed at much lower costs but this goes along with a less defined nanostructured surface and, as a consequence, much broader plasmonic resonance. In Figure 1 B the coral like structure of an electrochemically roughened Ag electrode can be seen. The surface roughness can be approximated by a random nanostructure. For such systems an almost continuous surface enhancement is predicted over the entire optical range (Sanchez-Gil & Garcia-Ramos, 1998). Surprisingly the SERR intensity of heme proteins adsorbed on these surfaces is quite reproducible. Nevertheless it is not possible to determine which part of the surface is responsible for the obtained SERR intensity. It might very well be that the measured signal is achieved from a small fraction of proteins localised so called *hot spots*, which are parts of the surface that provide extremely high surface enhancement (Moscovits, 2005).
Biocompatible surface functionalisation of roughened Ag electrodes can be achieved by exposing the electrode to a solution containing ω-functionalised mercaptoalkanes for several hours. The choice of the SAM´s solvent exposed headgroup as well as proper adjustment of buffer solution parameters have a strong influence on the protein's adsorption efficiency but also on its electrochemical and catalytic performance on the surface. We will demonstrate this on two different heme proteins; *iso-1-yeast cytochrome c* (YCyt *c*) and *human sulfite oxidase* (HSO):

YCyt *c* is very similar to *horse heart cytochrome c* (HCyt *c*), which is more commonly used in (spectro-)electrochemical studies and which is generally referred to as simply Cyt *c*. Although both proteins exhibit the same functionality in their respective environments, they show significantly different adsorption behaviour on electrodes due to their different dipole moments (536 D for ferrous YCyt *c* against 150 D for HCyt *c*, Feng et al., 2008) and the fact that YCyt *c* possesses a single surface cysteine on position 102.
HSO on the other hand is an enzyme that catalyses the oxidation of sulphite to sulphate, which is the terminal reaction in the oxidative degradation of the sulphur-containing amino acids cysteine and methionine (Garrett et al., 1998). HSO contains three sub-domains. The large central domain harbours the catalytic center, made of a *molybdopterin* cofactor (Moco) . This domain is connected via a flexible loop region to a heme containing *cytochrome b*5 (Cyt *b*5) domain. The third domain is responsible for binding to a second HSO monomer and is thus called the dimerisation domain. Catalytic sulphite oxidation takes place at the Moco domain followed by a fast intramolecular electron transfer to the heme center. From there the electron is transferred to an external redox partner.
At ambient pH YCyt *c* exhibits a positive net charge while the Cyt *b5* domain of HSO is negatively charged. Thus the choice of charge at the solvent exposed headgroup can promote adsorption of either one or the other protein.

3.2.1 Selective protein binding

High quality SERR spectra of YCyt *c* are obtained on rough Ag electrodes coated with negatively charged carboxyl-terminated SAMs (Figure 4 A). The same electrode can be made repulsive for YCyt *c* if positively charged amino-terminated SAMs are used. In this case the recorded spectrum shows no sign of protein binding (Figure 4 B).

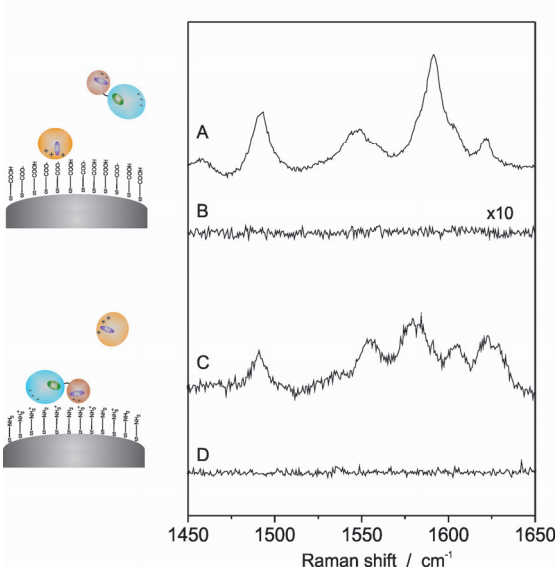

Fig. 4. SERR spectra of YCyt *c* (A,D) and HSO (B,C) on carboxyl (A,B) or amino (C,D) terminated SAMs. On the right side the selective binding of each protein to the respective SAM is shown schematically.

An inverse behaviour is observed for HSO, where only on amino terminated SAMs a SERR spectrum can be recorded (Figure 4 C,D). The heme is in both proteins differently coordinated as the 6th ligand is a methionine for YCyt *c* and a histidine for HSO. This difference can most accurately be monitored by the characteristic vibrational pattern of the respective ferric species in the region between 1450 and 1650 cm^{-1}. Both proteins can therefore easily be distinguished.

3.2.2 Redox properties and electron transfer dynamics

The electron transfer properties of redox proteins on surfaces are strongly influenced by the binding strength of the protein to the SAM and hence are a function of the local charge density at the SAM/protein interface (Ly et al., 2011). If the charge density of the SAM headgroup is too high the flexibility of the protein is largely restrained which can lead to a significant decrease of the redox rate k_{redox}. If the electrostatic dipole-dipole interaction between the SAM coated electrode and the protein exceeds a certain level also irreversible damage to the protein's 3D structure can occur. Depending on the protein´s dipole moment the threshold for harmful charge density can be reached at different levels. This effect is shown exemplarily for HCyt *c* and YCyt *c*: HCyt *c* can be immobilised on pure carboxyl-terminated SAMs under preservation of the native structure and redox activity (k_{redox} = 50 s^{-1} Ly et al., 2011b). The same immobilisation conditions, however, are not appropriate for YCyt *c* for which, due to its higher dipole moment, no redox activity and a slow denaturation process is observed when immobilised on pure MUA SAMs at pH 7 (Feng et al. 2008). The charge density at the SAM/protein interface can be decreased if a lower pH is adjusted and/or if the carboxyl-terminated SAM is mixed with OH terminated mercaptoalkanes. At pH 6 protein denaturation is suppressed and the protein remains redox active on the surface albeit with a ten times lower electron transfer rate compared to HCyt *c* (table 1). The same desired tendency is achieved by mixing MUA with mercaptoundecanol (MU) or mercaptohexanol (MH) which both promote an increase in redox rate. In all cases a better performance is observed at pH 6 compared to pH 7.

SAM	k_{redox} / s^{-1}	
	pH 7	pH 6
MUA	n.d	5.2
MUA/MU	4.8	7.5
MUA/MH	8.6	18

Table 1. Effect of pH and SAM composition on the apparent redox rate of YCyt *c*.

The local charge density is expected to have an even stronger impact if the direction of the protein´s dipole moment is significantly different from the direction of the most efficient electron transfer pathway. This is the case for HSO where the Cyt *b5* domain acts as an electron mediator between the catalytic Moco site and the electrode. HSO forms dimers via the dimerisation sub domain. Dipole moment calculations revealed that the HSO dimer most likely binds via this dimerisation domain to amino terminated SAMs. Under low ionic strength conditions (5 mM Tris acetate buffer) also the Cyt *b5* domain is bound directly to the SAM (See cartoons in Figure 5). The Cyt *b5* adsorption is driven by electrostatic forces and will therefore occur in the direction of the protein's dipole moment which is in this case not favourable for electron transfer.

I / mM	E_0 / V	k_{redox} / s^{-1}	k_{cat} / s^{-1}
5	-0.05	17	
150	-0.11	220	1.6
500	-0.11	340	
750	-0.11	440	5.3

Table 2. Effect of ionic strength on the redox properties of HSO. Immobilisation is done on a C8(NH_2)/C6(OH) SAM in tris acetate buffer at pH 7.4. Midpoint potentials refer to the Ag/AgCl reference electrode.

Increasing the ionic strength allows rotational diffusion of the protein on the surface which leads to a significant increase in redox rate (Table 2). The highest change in redox rate though is observed between 5 mM and 150 mM buffer concentration which is accompanied by a change in the Cyt *b5* midpoint potential E_0 from -0.05 V to -0.11 V (Sezer et al., 2010b). The latter value is similar to the one measured in solution. Further increase of the ionic strength leads to an increase in redox rate but does not alter the midpoint potential. Shifts in midpoint potential in respect to its value in solution can be associated with the formation of a strongly bound SAM/protein complex (Murgida & Hildebrandt, 2001). Hence we can say that for ionic strength > 150 mM direct electrostatic attraction between the Cyt *b5* domain and the SAM surface has been mostly eliminated. This interpretation is supported by the fact that the isolated Cyt *b5* domain irreversibly desorbs if buffers with ionic strengths > 50 mM are used.

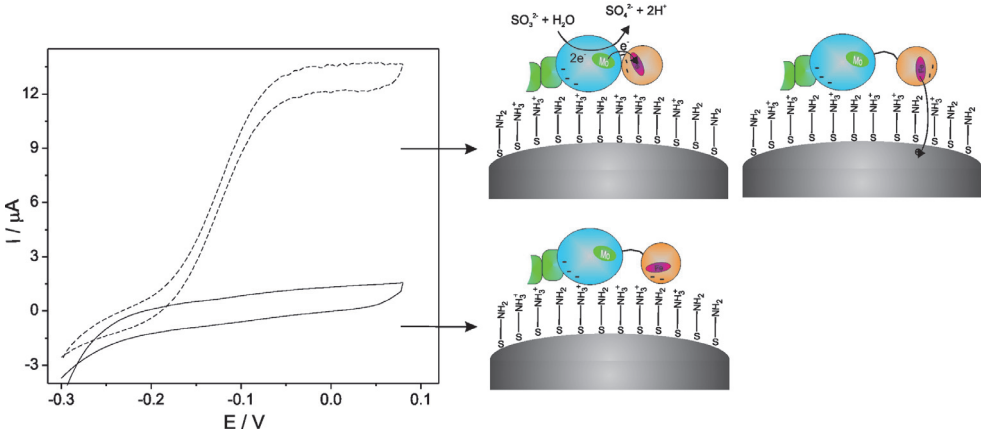

Fig. 5. Cyclo-voltammetric measurements of HSO on electrodes in the presence of low (solid line) and high (dashed line) ionic strength. On the right side the respective molecular electron transfer mechanisms is drawn schematically. At high ionic strength (top) the Cyt *b5* domain is able to rotate on the electrode. At low ionic strength (bottom) the Cyt *b5* domain is fixed on the SAM surface in direction of its dipole moment which is not favourable for electron transfer.

Flexibility of the Cyt *b5* domain is required even more for its functioning during catalysis. In the presence of substrate the electrons that are catalytically generated through substrate oxidation have to be transferred from the Moco site to the heme of the Cyt *b5* domain and

from there to the electrode. The rate of catalytic sulphite oxidation k_{cat} can be determined from protein film voltammetry (PFV) (Sezer et al., 2010b) by:

$$k_{cat,el} = \frac{I_{\lim} \cdot \nu \cdot n \cdot F}{I_a \cdot 4 \cdot R \cdot T} \quad (3)$$

I_a is the current of the redox peak under non-turnover (no substrate present) conditions. $I_{\lim}$ is the maximum current under turnover conditions when substrate mass transport to the protein can be excluded. *F* and *R* are the Faraday and molar Gas constant respectively. ν is the scan rate and *n* denotes the number of transferred electrons.

In order to get efficient catalytic turnover rates, experimental conditions have to be optimised in respect to both the intramolecular- and the heterogeneous electron transfer rates. This requires that the Cyt *b5* domain has to switch forth and back between the Moco binding patch and the SAM surface, which is only possible if electrostatic interaction between the Cyt *b5* domain and the SAM is kept to a minimum. In this respect in makes sense that, as observed, no catalytic activity is observed under low ionic strength conditions (Figure 5) but a steady increase in k_{cat} arises as the ionic strength is increased (Figure 5 and table 2).

3.3 Hybrid Ag-Au systems

In the system described in section 3.2 Ag electrodes function as both, optical amplifier and redox partner. While optical amplification is unambiguously preferred for Ag its chemical properties are rather poor as Ag is generally assumed to be bio-incompatible and easy to oxidise. In this respect Au is preferable since it is inert and its higher thiol affinity works in favour of well defined organic layer formation by mercaptoalkane derivatives. However, Au is not capable to provide surface enhancement at wavelengths lower than 520 nm. Ag-Au hybrid electrodes where optical amplification is provided by Ag but surface reactions take place at an Au surface could be able to combine the advantages of both metals. Hence we describe a procedure to create such multilayered hybrid supports and discuss the parameters that are responsible for the optical and chemical performance of the device in respect to bioelectronic applications:

The first layer consists of a rough Ag electrode as described in section 3.2. In order to minimise the contact between the biomolecule and the Ag surface a dielectric spacer (*S*) by either an amino terminated SAM (Feng et al., 2009) or a thin silica film (Feng et al., 2010) is applied to the rough Ag electrode. In the latter case the SiO_2 surface is further functionalised with NH_2 groups by exposing the SiO_2 coated electrode to a solution containing *aminopropyl triethoxysilane* (APTES). This layer not only prevents Ag from reacting with biological surface species it also passivates the surface for molecules with a positive net charge. Interestingly this layer also improves the optical performance of the device which is described in more detail in section 3.3.2.

Finally an Au island film is formed on top of the *Ag-S* electrode by electrochemical reduction of $AuCl_4^-$ ions from solution. A schematic setup of the electrode can be seen in Figure 6. The morphology of the Au island film differs from the nanostructure of the underlying Ag support as can be seen in figure 1 C which shows a cut through the Ag-S-Au electrode. The thickness of the Au film can be controlled by the exposure time of the electrode in the $AuCl_4^-$ solution.

3.3.1 Protein binding strategies

Cyt *c* is used again as a model protein to test the optical and chemical performance of Ag-S-Au electrodes. For a direct comparison with Ag electrodes under biocompatible conditions the Au surface is additionally functionalised with MUA. In this case the Cyt *c* Raman signal can be directly attributed exclusively to proteins bound to the Au-MUA surface as the protein will not bind to amino groups from the dielectric spacer that is in contact with the solution (see Figure 4 D). The SERR intensity of Cyt *c* bound to the MUA coated Au surface is at 413 nm excitation only slightly lower than in the case of pure Ag-MUA electrodes (Feng et al., 2009). This result is quite remarkable as Au is not plasmonically active under violet light excitation and the distance between Cyt *c* and the amplifying Ag support has been significantly enlarged. A more detailed description of the mechanism that lies behind this phenomenon will be given in section 3.3.2.

The electrical communication between Cyt c bound to the Au islands and the working electrode remains generally intact which makes it possible to perform redox titrations by potential controlled SERR spectroscopy. In Figure 6 C the molar fractions of the reduced and oxidised Cyt c species as a function of applied potential are shown. A sharp redox transition can be seen at the characteristic potential for the native MUA bound Cyt *c*. Only small differences in the midpoint potential between Ag (20 mV *vs.* Ag/AgCl Ly et al., 2011b) and Ag-S-Au (4 mV *vs.* Ag/AgCl) are observed for this electrostatic immobilisation strategy.

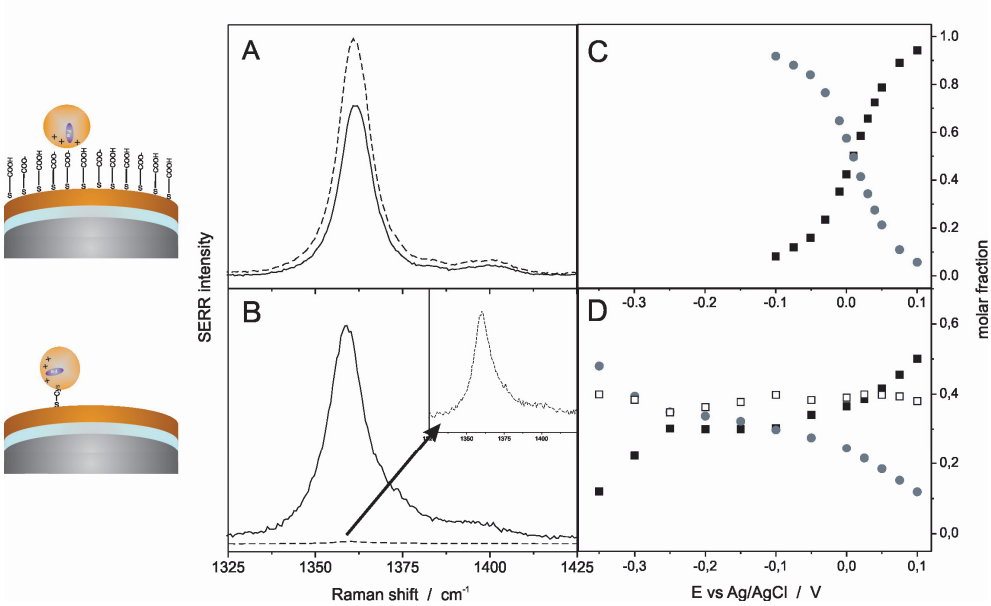

Fig. 6. SERR spectra of the ν_4 region of (A) Cyt c electrostatically bound to MUA coated electrodes or (B) YCyt *c* covalently bound via Cys 102. SERR spectra were recorded on Ag (dashed line) and Ag-S-Au (solid line) surfaces. (C,D) Molar fraction of the native reduced (grey circles), native oxidised (solid squares) and non native oxidised (open squares) species of YCyt *c*. Inset in figure 5B shows the 100 times amplified YCyt c spectrum on Ag. On the left side the type of binding on Ag-S-Au electrodes is illustrated.

In contrast drastic differences for Ag and Au supports can be observed for immobilisation strategies that include direct thiol binding of proteins via cysteine residues. YCyt *c* contains a single surface cysteine at position 102 that binds covalently to Au surfaces under preservation of its native redox properties, as concluded from electrochemical investigations (Heering et al., 2004). However, SERR measurements of YCyt *c* using the same immobilisation strategy on Ag surfaces yield only very weak protein loading which we attribute to the comparably low thiol affinity of Ag in comparison with Au. The Raman signal is in this case too low for SERR spectroscopic investigations (see figure 6 B). In contrast YCyt *c* bound via Cys102 to Au in Ag-S-Au electrodes gives a more than 100 times higher Raman signal and thus potential dependent SERR spectroscopy can be performed. The electrochemical findings can partially be confirmed as for the Cys 102 bound YCyt c a redox transition is observed, which means that the electrical communication remains *per se* intact using this immobilisation strategy. However, a large fraction of the proteins show the vibrational features of a non-native 5c high spin state. This fraction remains redox inactive on the surface (Figure 6 D).

3.3.2 Parameters for optical amplification in multilayerd systems

In this section the parameters that are responsible for surface enhancement at the Au surface in Ag-S-Au electrodes are discussed in more detail.

If one takes a hybrid electrode with a dielectric spacer of *11-amino-1-undecanethiol* (AUT, 2 nm) and a 10 nm average Au film thickness the additional layers will enlarge the distance between the Cyt c Raman marker and the SER active Ag surface by roughly 12 nm. If one uses equation 2 with a_0=40 nm as a first approximation the Raman signal of Cyt *c* bound to Ag-S-Au-MUA should be by a factor 20 smaller as compared to pure Ag-MUA. Interestingly, the measured Raman intensity of Cyt c shown in Figure 6 A only decreases by a factor 1.2. We attribute this effect to a long range plasmon coupling between the free electron gas of Ag and Au although the latter metal can not enhance the incoming light by itself. This plasmon coupling leads to an induced plasmonic vibration of the Au electron gas resulting in a field enhancement at the Au surface.

A crucial role for the magnitude of the induced enhancement in such multilayered systems is played by the dielectric spacers that are placed in between and on top of the metal films. These two dielectric layers will be referred as the *inner* and *outer* layer. In the following Raman surface enhancement *REF* will be calculated as a function of thickness of the respective layers.

For the enhancement factor directly at the Ag surface we adopt the value of $EF(0)= 8 \cdot 10^4$ at 413 nm excitation from AgNP aggregates (Hildebrandt & Stockburger 1986). Correlation of this enhancement factor to measured Cyt *c* SERR intensities is difficult since Cyt *c* bound directly to Ag will be denaturated which goes along with a signal decrease as a function of time. Therefore the much more stable SERR signal of Cyt *c* bound to MUA coated electrodes is used as a reference. MUA has a layer thickness of 1.9 nm. Applying equation 2 and assuming a_0=40 nm the Raman intensity of Cyt c should have been decreased in that distance by a factor of 2.5 corresponding to an enhancement factor of $EF = 3 \cdot 10^4$ at the MUA interface. Enhancement factors for different layer systems are derived in respect to this value on the basis of measured Cyt c ν_4 SERR intensity (Figure 7). According to equation 2 the distance dependence of log(EF) is approximately linear and can be described by $\Delta\log(EF) = 0.1\ nm^{-1}$. In the experiment, one would expect to observe similar distance dependence by variation of the inner and outer layer thickness. The outer layer thickness can be changed by

using SAMs of different alkane chain length. For Ag-S-Au systems this leads to a value of $\Delta\log(REF) = 0.11\ nm^{-1}$ (Figure 7 A) which fits nicely to the theory. For SAM coated Ag electrodes a much stronger dependence on SAM thickness ($\Delta\log(EF) = 0.53\ nm^{-1}$) and a less linear characteristic was found (Murgida & Hildebrandt, 2001).
Variation of the thickness of the inner dielectric layer in Ag-S-Au systems reveals a different behaviour: Here a very weak distance dependence of $\Delta\log(EF) = 0.02\ nm^{-1}$ is determined from measurements with SiO_2 coatings of different thickness (Figure 6 B). Most likely this discrepancy from the theory occurs due to the fact that the inner spacer layer is situated between two metals (Ag and Au). Such an effect was observed in calculations for spherical Ag-SAM-Au core shell particles (David et al., 2010) and most likely can be transferred to nanostructured layered devices. For practical applications in SERR spectroscopy of biomimetic systems this result can have an enormous impact, since it allows separating sensitive biological probes from harmful optical amplifiers much more than so far expected from theory.

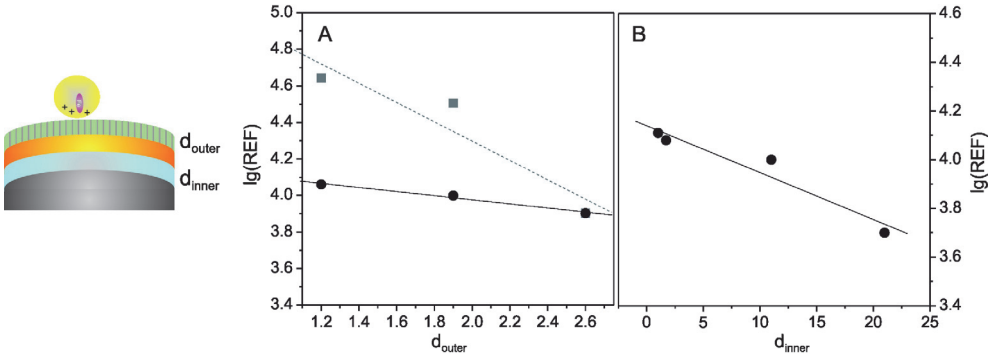

Fig. 7. Logarithmic Raman enhancement factors as a function of (A) inner and (B) outer spacer thickness for Ag-S-Au-SAM (black) and Ag-SAM (grey) electrodes. On the left side the different layers of the Ag-S-Au-SAM electrode are illustrated.

3.3.3 Electron transfer properties

In section 3.3.1 it was shown that Cyt c bound to Au surfaces in Ag-S-Au devices still has an intact electrical communication. We will further analyse this aspect by comparing the redox rates of Cyt *c* on single- and multilayered electrodes. In the latter case also the electron transport through the inner layer has to be taken into consideration. The results indicate that rather the material of the dielectric spacer layer than its thickness is crucial for a fast electron transport through the layer. While electron transfer is significantly slowed down for systems having SiO_2 as an inner spacer layer the redox rates of Cyt *c* on Ag-AUT-Au-SAM systems is at least comparable, in some cases even faster, to the ones measured on Ag-SAM (Sezer et al., 2011). If the electron transfer rate through the inner layer is comparably fast, the measured redox rates depend only on the electron tunnelling probability through the outer layer. This is the case if MUA or MHDA (*16-mercaptohexadecanoic acid* $HS(CH_2)_{15}COOH$) are used as outer SAMs. For potential jumps to the midpoint potential (i.e. at zero driving force) the redox rates of Cyt *c* on MUA are comparable in Ag and Ag-AUT-Au systems (Table 3), which indicates that the multilayer structure of the Ag-AUT-Au electrode does not slow

down the electrical communication. If MHDA is used as outer layer a more than 4 times faster rate is measured on Ag-AUT-Au electrodes. On first hand this result may be very surprising, but it is in line with the general observation that the Cyt *c* redox process is faster on Au than Ag (Wisitruangsakul et al., 2008) due to the following reasons:
First, the tilt angle with respect to the surface normal is higher on gold (~ 30° (Porter et al., 1987)) as compared to silver (~15°, Laibinis et al., 1991), which results in a slightly shorter tunnelling distance for electrons through SAMs on Au surfaces.
Second the potential of zero charge E_{PZC} is different for both metals. The difference between the applied potential and the potential of zero charge $\Delta E = E\text{-}E_{PZC}$ influences the charge density of the metal and hence also the deprotonation grade of the COOH/COO- SAM. It is thus, directly and indirectly, responsible for the electric field strength at the SAM/protein interface. On Ag-MUA we measured a value of E_{PZC}=-0.45 V (Feng et al., 2008) whereas on Au-MUA E_{PZC} = 0 V was determined (Ramirez et al., 2007). The latter value is close to the Cyt *c* midpoint potential, hence redox processes on Au take place under lower electric field strength than on Ag. Thus proteins on Au-SAM surfaces exhibit a higher flexibility, which, as we have already shown in section 3.2.2, promotes a fast electron transfer.
If we assume that the use of MHDA instead of MUA does not change the overall trend in E_{PZC} of SAM coated Ag and Au surfaces, both effects are most likely responsible for the faster rates observed on Ag-AUT-Au-MHDA as compared to Ag-MHDA (table 3). However, in this case a modification of E_{PZC} in respect to pure Au surfaces has to be considered since Ag indirectly influences the charge density on the gold island film. We have indeed measured a value of ca. E_{PZC}=-0.2 V for Ag-AUT-Au-MUA systems (Sezer et al., 2010) which lies between the two values of the respective pure metals.
The driving force for the electron transfer process can be increased by applying a higher overpotential η, which is defined as the difference between the applied potential *E* and the midpoint potential E_0 of the respective redox protein (Ly et al., 2010b; Murgida & Hildebrandt, 2002). As a consequence the redox rates k_{redox} of Cyt c increase as a function of η for both, single and multilayered systems (Table 3). It has to be noted that k_{redox} remains faster for the multilayered system with MHDA as outer layer also at higher overpotentials.
For MUA used as outer SAM the redox rates of Cyt *c* on Ag-AUT-Au-MUA are falling behind Ag-MUA at higher overpotential. Most likely this is related to the growing influence of the electron tunnelling rate through the inner spacer layer which clearly demonstrates the limitation of multilayered electrodes.

	MHDA		MUA	
η	k_{redox}(Ag) / s^{-1}	k_{redox} (Ag-AUT-Au) / s^{-1}	k_{redox} (Ag) / s^{-1}	k_{redox} (Ag-AUT-Au) / s^{-1}
0	0.15	0.8	53	45
-0.05	0.3	1.2		
-0.1	0.6	1.2	240	
-0.2	1.5	4.9	320	167
-0.3	2.9	8.2	370	
-0.4	3.7	9.0	500	313
-0.6	3.9	9.6		

Table 3. Redox rates k_{redox} of Cyt c on Ag and Ag-AUT-Au electrodes as a function of applied overpotential $\eta = E\text{-}E_0$ using MUA and MHDA respectively as outer dielectric layers.

Nevertheless for MHDA as outer layer the redox dynamics is clearly limited by the electron tunnelling rate through the outer layer and hence can be analysed in respect to heterogeneous electron transfer theory. In order to determine the electron transfer rate from measured redox rates, the contribution of the back reaction has to be taken into account. At zero driving force (η = 0 V) we have k_{ET}(forth) = k_{ET}(back) and hence k_{ET} = k_{redox}/2. For higher driving forces we neglect the back reaction and set k_{redox} = k_{ET}.

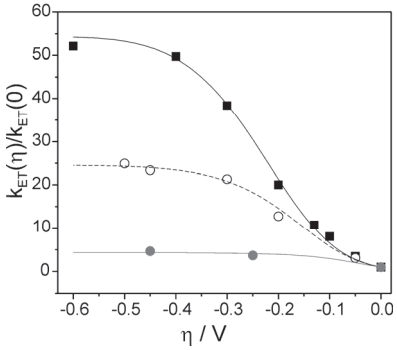

Fig. 8. Rates for $k_{ET}(\eta)/k_{ET}(0)$ as a function of overpotential for Ag-MHDA (black squares), Ag-AUT-Au-MHDA (open circles) and Au-MHDA (solid circles) electrodes together with a fit using equation 4, 5 and 6.

In order to elucidate the role of the metal support in electron transfer reactions the measured values of $k_{ET}(\eta)/k_{ET}(0)$ are plotted in figure 8 as a function of overpotential for Ag-MHDA and Ag-S-Au-MHDA electrodes together with results from Au-MHDA from SEIRA (*surface enhanced infrared adsorption spectroscopy*) measurements (Wisitruangsakul et al., 2008; Ly et al., 2011b). The dependence of $k_{ET}(\eta)/k_{ET}(0)$ as a function of η clearly decreases in the order Ag > Ag-Au > Au. The increase in electron transfer as a function of driving force can be quantitatively described from electrochemical electron transfer theory (Nahir et al., 1994; Murgida & Hildebrandt, 2002):

$$\frac{k_{ET}(\eta)}{k_{ET}(0)} = \frac{erfc\left(\frac{\lambda + e\eta}{\sqrt{4\lambda k_B T}}\right)}{erfc\left(\frac{\lambda}{\sqrt{4\lambda k_B T}}\right)} \tag{4}$$

where k_B and T stand for the Boltzmann constant and temperature respectively. λ denotes the reorganisation energy of the redox process. On the basis of equation 4 the data for Ag-MHDA was previously fitted with a reorganisation energy of λ= 0.22 eV (Murgida & Hildebrandt, 2002). The same approach for multilayered Ag-Au systems yields a lower value of λ = 0.15 eV. For Au λ would approach a value close to zero. It is highly unlikely that the reorganisation energy is so drastically altered by the support material. Hence these findings can only be rationalised by considering a dependence of the electron transfer on the magnitude and sign of the metal charge, which, given their different potential of zero charge, will be different for Ag, Ag-AUT-Au and Au in the investigated potential range.
The data in figure 8 suggests that a process other than electron tunnelling becomes rate limiting if the applied potential is more negative than E_{PZC}. To quantitatively describe this

effect we assume that we measure an apparent electron transfer rate k'_{ET} that consists of two individual rates: The first rate (k_{ET}) corresponds to the heterogeneous electron transfer rate described by equation 4 and depends on the applied potential E and the the midpoint potential E_0. The second rate (k_C) is a function of the potential of zero charge (E_{PZC}). k'_{ET} is then a function of E, E_0 and E_{PZC} and can be written as:

$$\frac{1}{k'_{ET}(E,E_0,E_{PZC})} = \frac{1}{k_{ET}(E,E_0)} + \frac{1}{k_C(E_{PZC})} \tag{5}$$

The functional dependence of k_C on E_{PZC} is not known. However if we assume in a first approximation that

$$k_C(E_{PZC}) = k_{ET}(E_{PZC},E_0) \tag{6}$$

a good fit to the measured $k_{ET}(\eta)/k_{ET}(0)$ values for all 3 systems is obtained using λ=0.29 eV and the independently determined E_0 values of Cyt c on the respective metals (Table 4). The values for E_{PZC} were initially taken from the E_{PZC} measurements on MUA coated electrodes. and were slightly modified for Ag and Au electrodes to obtain the best fit to the data (Figure 8). We note that a fundamental interpretation of k_C is missing in this approach, a more quantitative description, however, would require a more elaborate description of the interfacial electric field and its influence on the monolayer which is beyond the scope of the present work.

	E_0	E_{PZC}(fit)
Ag	0.006	-0.41
Ag-AUT-Au	0.015	-0.2
Au	0.03	-0.03

Table 4. Midpoint potential E_0 of Cyt c on Ag ,Ag-AUT-Au and Au electrodes, using MHDA SAMs as outer layer, and potential of zero charge E_{PZC} of the respective supports determined from equations 4, 5 and 6.

3. Conclusion

In this book chapter different plasmonic support materials were described in respect to their applicability for biomimetic systems. Fine tuning of the optical amplification parameters allows employing *Surface enhanced resonance Raman spectroscopy* for monitoring the structural state of selected protein cofactors during biological surface reactions. Several heme containing enzymes, immobilised on functionalised Ag-nanoparticles, -electrodes and Ag-Au multilayer supports, are used as Raman markers and biological redox probes in order to find conditions for high signal intensity together with good device performance.

The highest control over frequency dependent optical amplification is achieved with nanoparticles, which are designed for selective enhancement of protein heme cofactors in solution. Biocompatible coatings can be applied to the particles on the expense of SERR intensity but with a significant gain in protein structure preservation.

While those nanoparticles provide a very flexible tool to enhance specific cofactors in solution or on biological interfaces, the study of redox processes additionally requires simultaneous control of the supports electrical potential. This is achieved using nanostructured Ag electrodes or newly developed Ag-S-Au supports. The latter have Ag as a bulk support and Au as solution facing reaction surface and thus combine the broad

optical amplification properties of Ag with the superior chemical characteristics of Au. The multilayer structure of the Ag-S-Au hybrid supports allows furthermore increasing the distance of the protein from the harmful Ag surface without loosing significant Raman signal intensity.
It is further demonstrated how the change of the interfacial conditions can increase electrical communication and catalytic efficiency of immobilized proteins while at the same time sufficient signal enhancement is provided for spectroscopic analysis. It turns out that, rather than the amount of immobilised protein, its flexibility on the surface is crucial for the electron transfer and catalytic performance of the device. Protein flexibility on SAM coated metal surfaces can be influenced by adjusting the local charge distribution at the Protein/SAM interface as demonstrated i.e. by the increase in electron transfer rate of HSO as a function of buffer ionic strength. Also the choice of metal support can be crucial for the electrical performance of biomimetic devices as different metals i.e., Ag, Au and Ag-S-Au, show a different electron transfer rate dependence on the applied overpotential. This different behaviour is attributed to a yet not fully understood electric field dependence arising from the metal specific potential of zero charge.

4. Acknowledgment

We would like to thank Peter Hildebrandt for his great support and Alois Weidinger for last minute corrections. Financial support by the Fonds der Chemie, the DFG (Unicat) and the National Science Foundation of China (J.J.F.; NSFC No. 20905021) is gratefully acknowledged. Big thanks also to our colleagues Khoa Ly, Jacek Kozuch, Diego Millo and Anna Fischer who contributed to this work.

5. References

Bain, C.D.; Troughton, E.B.; Tao, Y.T.; Evall, J.; Whitesides, G.M. & Nuzzo, R.G. (1989). Formation of monolayer films by the spontaneous assembly of organic thiols from solution onto gold. *Journal of the American Chemical Society*, Vol.101, No.1, pp. 321–335

Bonifacio, A.; van der Sneppen, L.; Gooijer, C. & van der Zwan, G. (2004). Citrate-reduced silver hydrosol modified with omega-mercaptoalkanoic acids self-assembled monolayers as a substrate for surface-enhanced resonance Raman scattering. A study with cytochrome c. *Langmuir*, Vol. 20, No.14, pp. 5858-5864

David, C.; Richter, M.; Knorr, A.; Weidinger, I. M. & Hildebrandt, P. (2010). Image dipoles approach to the local field enhancement in nanostructured Ag-Au hybrid devices. *Journal of Chemical Physics,* Vol. 132, pp.024712

Feng, J.J.; Gernert, U. ; Hildebrandt, P. & Weidinger, I.M. (2010). Induced SER-Activity in Nanostructured Ag-Silica-Au Supports via Long Range Plasmon Coupling. *Advanced functional Materials,* Vol.20, No.12, pp. 1954-1961

Feng, J.J.; Gernert, U. ; Sezer, M.; Kuhlmann, U.; Murgida, D.H.; David, C.; Richter, M. ; Knorr, A.; Hildebrandt, P. & Weidinger, I.M. (2009). A Novel Au-Ag hybrid device for surface enhanced (resonance) Raman spectroscopy. *Nano Letters* Vol. 9, pp. 298-303

Feng, J.J.; Murgida, D.H.; Utesch, T.; Mroginski, M.A.; Hildebrandt, P. & Weidinger, I.M. (2008). Gated electron transfer of yeast iso-1 cytochrome c on SAM-coated electrodes. *Journal of Physical Chemistry B* Vol. 112, pp.15202–15211

Garrett, R. M. ; Johnson, J. L.; Graf, T. N.; Feigenbaum, A. & Rajagopalan, K. V. (1998). Human sulfite oxidase R160Q: identification of the mutation in a sulfite oxidase-deficient

patient and expression and characterization of the mutant enzyme. *Proceedings of the National Academy of Sciences United States of America*, Vol.95, No.11, pp. 6394

Haynes, C. L. & Van Duyne, R. P. (2001). Nanosphere lithography: A versatile nanofabrication tool for studies of size-dependent nanoparticle optics. *Journal of Physical Chemistry B,* Vol.105, pp. 5599-5611

Heering, H. A.; Wiertz, F. G. M.; Dekker, C., & de Vries, S. (2004). Direct immobilization of native yeast Iso-1 cytochrome c on bare gold: Fast electron relay to redox enzymes and zeptomole protein-film voltammetry. *Journal of the American Chemical Society,* Vol.126, pp. 11103-11112

Hildebrandt, P. & Stockburger, M. (1986). Surface-Enhanced Resonance Raman-Spectroscopy of Cytochrome-C at Room and Low-Temperatures. *Journal of Physical Chemistry,* Vol.90, pp. 6017-6024

Jana, N. R.; Gearheart, L. & Murphy, C. J. (2001). Seeding Growth for Size Control of 5−40 nm Diameter Gold Nanoparticle. *Langmuir*, Vol. 17, No.22, pp.6782-6786

Jeanmaire, D. L. & Vanduyne, R. P. (1977). Surface Raman Spectroelectrochemistry .1. Heterocyclic, Aromatic, and Aliphatic-Amines Adsorbed on Anodized Silver Electrode. *Journal of Electroanalytical Chemistry,* Vol.84, pp. 1-20

Kelly, K. L., Coronado, E., Zhao, L. L., & Schatz, G. C. (2003). The optical properties of metal nanoparticles: The influence of size, shape, and dielectric environment. *Journal of Physical Chemistry B,* Vol.107, pp. 668-677

Lal, S., Grady, N. K., Kundu, J., Levin, C. S., Lassiter, J. B., & Halas, N. J. (2008). Tailoring plasmonic substrates for surface enhanced spectroscopies. *Chemical Society Reviews,* Vol.37, pp. 898-911.

Laibinis, P. E.; Whitesides, G. M.; Allara, D. L.; Tao, Y. T.; Parikh, A. N. & Nuzzo, R. G. (1991). Comparison of the structures and wetting properties of self-assembled monolayers of normal-alkanethiols on the coinage metal surfaces, Cu, Ag, Au. *Journal of the American Chemical Society,* Vol.113, pp.7152 – 7167

Link, S. & El-Sayed, M. A. (1999). Spectral properties and relaxation dynamics of surface plasmon electronic oscillations in gold and silver nanodots and nanorods. *Journal of Physical Chemistry B,* Vol.103, pp. 8410-8426

Ly, H.K.; Sezer, M.; Wisitruangsakul, N.; Feng, J.J.; Kranich, A.; Millo, M.; Weidinger, I.M.; Zebger, I.; Murgida, D.H. & Hildebrandt, P. (2011). Surface enhanced vibrational spectroscopy for probing transient interactions of proteins with biomimetic interfaces: electric field effects on structure, dynamics, and function of cytochrome. c, *FEBS Journal,* doi:10.1111/j.1742-4658.2011.08064.x

Ly, K.H.; Wisingtruangsakul, N.; Sezer, M.; Feng, J.J.; Kranich, A.; Weidinger, I.M.; Zebger, I.; Murgida, H.D. & Hildebrandt, P. (2011). Electric field effects on the interfacial electron transfer and protein dynamics of cytochrome c. *Journal of Electroanalytical Chemistry,* doi:10.1016/j.jelechem.2010.12.020

Leger, C. & Bertrand, P. (2008). Direct Electrochemistry of Redox Enzymes as a tool for Mechanistic Studies. *Chemical Reviews*, Vol.108, pp.2379-2438

Le Ru, E.C. & Etchegoin, P.G. (2009). *Principles of Surface-Enhanced Raman Spectroscopy and related plasmonic effects*, ISBN 978-0-444-52779-0, Elsevier, Oxford, United Kingdom 2009

Moskovits, M. (2005). Surface-enhanced Raman spectroscopy: a brief retrospective. *Journal of Raman Spectroscopy* Vol.36, pp. 485-496

Murgida, D. H. & Hildebrandt, P. (2001). Heterogeneous electron transfer of cytochrome c on coated silver electrodes. Electric field effects on structure and redox potential. *Journal of Physical Chemistry B,* Vol.105, pp.1578-1586

Murgida, D. H. & Hildebrandt, P. (2002). Electrostatic-field dependent activation energies modulate electron transfer of cytochrome c. *Journal of Physical Chemistry B,* Vol.106, pp. 12814-12819

Nahir, T.M.; Clark, R. A. & Bowden, E. F. (1994). Linear-Sweep Voltammetry of Irreversible Electron Transfer in Surface-Confined Species Using the Marcus Theory. *Analytical Chemistry*, Vol.66 No.15, pp. 2595–2598

Oellerich, S., Wackerbarth, H., & Hildebrandt, P. (2002). Spectroscopic characterization of nonnative conformational states of cytochrome c. *Journal of Physical Chemistry B,* Vol.106, pp. 6566-6580

Porter, M. D.; Bright, T.B.; Allara, D.L. & Chidsey, C.E.D. (1987). Spontaneously organized molecular assemblies. 4. Structural characterization of n-alkyl thiol monolayers on gold by optical ellipsometry, infrared spectroscopy, and electrochemistry. *Journal of the American Chemical Society*, Vol.109, No. 12, pp. 3559–3568

Prodan, E., Radloff, C., Halas, N. J., & Nordlander, P. (2003). A hybridization model for the plasmon response of complex nanostructures. *Science,* Vol. 302, pp. 419-422

Ramirez, P., Andreu, R., Cuesta, A., Calzado, C. J., & Calvente, J. J. (2007). Determination of the potential of zero charge of Au(111) modified with thiol monolayers. *Analytical Chemistry,* Vol.79, pp.6473-6479

Sanchez-Gil, J. A. & Garcia-Ramos, J. V. (1998). Calculations of the direct electromagnetic enhancement in surface enhanced Raman scattering on random self-affine fractal metal surfaces. *Journal of Chemical Physics,* Vol.108, pp. 317-325

Sezer, M.; Feng, J.J.; Ly, H.K.; Shen, Y.; Nakanishi, T.; Kuhlmann, U.; Möhwald, H.; Hildebrandt, P. & Weidinger, I.M. (2010). Multi-layer electron transfer across nanostructured Ag-SAM-Au-SAM junctions probed by surface enhanced Raman spectroscopy. *Physical Chemistry Chemical Physics,* Vol. 12, No.33, pp. 9822-9

Sezer, M.; Spricigo, R.; Utesch, T.; Millo, D.; Leimkuehler, S.; Mroginski, M.A.; Wollenberger, U.; Hildebrandt, P. & Weidinger, I.M. (2010). Redox properties and catalytic activity of surface-bound human sulfite oxidase studied by a combined surface enhanced resonance Raman spectroscopic and electrochemical approach. *Physical Chemistry Chemical Physics;* Vol.12, No.28, pp. 7894-7903

Siebert, F. & Hildebrandt, P. (2008). *Vibrational Spectroscopy in Life Sciences*. ISBN 978-3-527-40506-0, Wiley-VCH, Weinheim, Germany 2009

Sivanesan, A.; Ly, H.K.; Kozuch, J.; Sezer, M.; Kuhlmann, U. ; Fischer, A. & Weidinger, I.M. (2011). Functionalized Ag nanoparticles with tunable optical properties for selective protein analysis. *Chemical Communications,* Vol. 47, pp. 3553-3555

Smith, W. E. (2008). Practical understanding and use of surface enhanced Raman scattering/surface enhanced resonance Raman scattering in chemical and biological analysis. *Chemical Society Reviews*, Vol.37, No.5, pp. 995-964

Tarlov, M.J. & Bowden, E.F. (1991). Electron Transfer Reaction of Cytochrome c Adsorbed on Carboxilic Acid Terminated Alkane Thiol Monolayer Electrodes. *Journal of the American Chemical Society* Vol. 113, pp. 1847-1849

Wisitruangsakul, N., Zebger, I., Ly, K. H., Murgida, D. H., Ekgasit, S., & Hildebrandt, P. (2008). Redox-linked protein dynamics of cytochrome c probed by time-resolved surface enhanced infrared absorption spectroscopy. *Physical Chemistry Chemical Physics, 10,* 5276-5286

Zeman, E. J. & Schatz, G.C. (1987). An Accurate Electromagnetic Theory Study of Surface Enhancement Factors for Ag, Au, Cu, Li, Na, Al, Ga, In, Zn, and Cd. *Journal of Physical Chemistry,* Vol. 91, pp. 634-643